JOURNAL OF SOLID STATE CHEMISTRY **141,** 587–593 (1998)
ARTICLE NO. SC988024

A Molybdenyl Chloromonophosphate with an Intersecting Tunnel Structure: $Ba_3Li_2Cl_2(MoO)_4(PO_4)_6$

M. M. Borel, A. Leclaire, J. Chardon, J. Provost, and B. Raveau

Laboratoire CRISMAT, UMR 6508 Associée au CNRS, ISMRA et Université de Caen, 6 Boulevard du Maréchal Juin, 14050 Caen Cedex, France

Received June 4, 1998; in revised form September 1, 1998; accepted September 9, 1998

A new molybdenyl chloromonophosphate, $Ba_3Li_2Cl_2(MoO)_4(PO_4)_6$, has been synthesized. It crystallizes in the space group $P2_12_12_1$, with $a = 9.1768(4)$, $b = 15.660(1)$, and $c = 18.117(2)$ Å. This original pseudotetragonal structure forms an intersecting tunnel framework $[Mo_4P_6O_{28}]_\infty$ built up from $[Mo_2P_2O_{12}]_\infty$ layers interconnected through single PO_4 tetrahedra. The $[Mo_2P_2O_{12}]_\infty$ layers derive from the perovskite structure by replacing one octahedron out of two by one PO_4 tetrahedron. The Li^+, Ba^{2+}, and Cl^- species are distributed in the [100], [001], [201], and [20$\bar{1}$] tunnels forming intersecting rows. Two sorts of polyhedra are found for Li^+: LiO_3Cl tetrahedra and LiO_3 triangular groups. The susceptibility measurements suggest a bidimensional antiferromagnetic behavior between 12 and 20 K, whereas a peak at 10 K is attributed to canting phenomena.

INTRODUCTION

The numerous studies performed recently on pentavalent molybdenum phosphates have shown the great ability of these compounds to form tunnel or layer structures in which large cations can be intercalated (see for a review, see Ref. (1)). Such an aptitude to generate an opened framework can be correlated to the chemistry of Mo(V), which implies a particular configuration of the MoO_6 octahedra. The latter must indeed possess one free apex, so that one observes molybdenyl ions which are only connected to voluminous cations.

Microporous solids are presently the aim of numerous investigations to get interesting catalytic properties. Besides the spectacular results obtained by hydrothermal synthesis (see, for instance, Ref. (2)), another direction of research would be to introduce, in tunnel or layer structures, anions as invited elements. For this reason, it is worth exploring the possibility of creating Mo(V) chlorophosphates to obtain larger cavities where chlorine would be introduced simultaneously with large cations. The recent synthesis of the Mo(V) chlorophosphate $AMoOClPO_4$ (A = K, Rb) (3) shows the possibility of creating a layer structure built up of $[(MoO)PO_4]_\infty$ layers between which are intercalated rock salt $[ACl]_\infty$ layers. In the present work, we describe a new Mo(V) chloromonophosphate, $Ba_3Li_2Cl_2(MoO)_4(PO_4)_6$, which exhibits an intersecting tunnel framework $[Mo_4P_6O_{28}]_\infty$, where Ba^{2+}, Li^+, and Cl^- species are interpolated.

EXPERIMENTAL

Crystal Growth and Chemical Synthesis

Single crystals of this new chlorophosphate were grown from a mixture of nominal composition $Ba_{5.5}Mo_8P_{12}O_{55}Li_{10}Cl_{10}$. This synthesis was performed in two steps: first an adequate mixture of MoO_3, $H(NH_4)_2PO_4$, and $BaCO_3$ was ground in an agate mortar and heated to 673 K in a platinum crucible for 1 h and then for 2 h at 873 K to liberate CO_2, NH_3, and H_2O. In a second step, the appropriate amounts of metallic molybdenum and lithium chloride were added and the finely ground mixture was sealed in an evacuated silica ampoule. The latter was heated for 24 h at 873 K, cooled to 8 K/h to 573 K, and finally quenched to room temperature. The result was a polyphasic sample in which several yellow plates were extracted. Microprobe analysis of several yellow crystals led to a Ba/Mo/P/Cl ratio 3/4/6/2, in agreement with the formula $Ba_3Mo_4P_6Cl_2Li_2O_{28}$. Atomic absorption analysis confirmed the expected lithium content (% Li = 0.85% observed for 0.92 calculated), in agreement with the structure refinements.

Attempts to prepare a single phase starting from the nominal composition $Ba_3Li_2Cl_2Mo_4P_6O_{28}$ were unsuccessful. They always led to a polyphasic sample. The major phase, which consisted of yellow crystals, was identified as the expected phase $Ba_3Li_2Cl_2Mo_4O_4(PO_4)_6$, whereas two minor phases—a red phase and a green phase—were identified respectively as $BaMo_4O_8(PO_4)_2$ (4) and $BaMo_2O_2(P_2O_7)_2$ (5).

Thus yellow crystals of the BaLi phase were picked out with tweezers using a binocular to perform magnetic characterization and to obtain their powder X-ray pattern.

0022-4596/98 $25.00

The latter was indexed in an orthorhombic cell with the parameters obtained from the single-crystal X-ray study.

Elemental Analysis

The analysis of molybdenum, chloride, phosphorus, and barium was performed with a Tracor microprobe mounted on a JEOL 840 scanning electron microscope. For the lithium analysis, the crystals were dissolved in a boiling aqueous solution of nitric acid ($\cong$6 N). The corresponding solution was analyzed by atomic absorption spectroscopy with a Varian AA20 spectrophotometer.

X-Ray Diffraction Study

Different crystals were examined by the Weissenberg method using Cu$K\alpha$ radiation. A yellow plate with dimensions $0.090 \times 0.077 \times 0.019\ mm^3$ was selected for the structure determination. Its cell parameters were determined by diffractometric techniques at 294 K with a least-squares refinement based on 25 reflections with $18^\circ < \theta < 22^\circ$. The data were collected on an Enraf-Nonius CAD4 diffractometer with the parameters reported in Table 1. The systematic extinctions, $h = 2n + 1$ for $h00$, $k = 2n + 1$ for $0k0$, and $l = 2n + 1$ for $00l$, are consistent with the space group

TABLE 1
Summary of Crystal Data, Intensity Measurements, and Structure Refinement Parameters for $Ba_3Li_2Cl_2Mo_4O_4(PO_4)_6$

1. Crystal data	
Cell dimensions	$a = 9.1768(4)$ Å
	$b = 15.660(1)$ Å
	$c = 18.117(2)$ Å
Volume	$V = 2603.6(3)$ Å^3
Space group	$P2_12_12_1$
Z	4
2. Data collection	
λ(Mo$K\alpha$)	0.71073 Å
Scan mode	ω–θ
Scan width (deg)	$1.0 + 0.35 \tan\theta$
Slit aperture (mm)	$1.0 + \tan\theta$
Maximum θ (deg)	45
Standard reflections	3 measured every hour
Measured reflections	11615 with $h,k,l \geq 0$
Reflections with $I > 3\sigma(I)$	2242
μ (mm^{-1})	7.02
3. Refinement	
Parameters refined	216
Agreement factors	$R = 0.040$
	$R_w = 0.034$
Weighting scheme	$w = 1/\sigma^2$
Δ/σ_{max}	0.0007
$\Delta\rho$(e Å^{-3})	− 2.70, 2.10

TABLE 2
Atomic Positional and Isotropic Displacement Parameters in $Ba_3Li_2Cl_2(MoO)_4(PO_4)_6$

Atom	X	Y	Z	U
Mo(1)	0.2168(2)	0.2060(1)	0.5016(1)	0.0050(5)
Mo(2)	0.2143(2)	0.30688(9)	0.2484(1)	0.0045(4)
Mo(3)	0.2144(2)	0.28010(9)	0.7486(1)	0.0042(4)
Mo(4)	0.2144(2)	0.2058(1)	0.0014(1)	0.0047(5)
Ba(1)	0.5057(2)	0.44828(9)	0.83150(7)	0.0158(3)
Ba(2)	0.4390(1)	0.01065(8)	0.40756(7)	0.0124(3)
Ba(3)	0.4239(2)	0.4674(1)	0.56691(8)	0.0322(5)
Cl(1)	0.1616(6)	0.0065(4)	0.3124(3)	0.020(1)
Cl(2)	0.1654(6)	0.5042(4)	0.4645(3)	0.026(1)
Li(1)	0.143(4)	0.050(2)	0.718(2)	0.012(7)
Li(2)	0.079(6)	0.410(3)	0.866(3)	0.06(2)
P(1)	0.4645(5)	0.2409(3)	0.6259(3)	0.006(1)
P(2)	0.4614(5)	0.2465(3)	0.3744(3)	0.006(1)
P(3)	0.4671(5)	0.2709(3)	0.1251(3)	0.003(1)
P(4)	0.4696(6)	0.2253(4)	0.8766(3)	0.006(1)
P(5)	0.1788(5)	0.4912(3)	0.7315(3)	0.007(1)
P(6)	0.3122(5)	0.0051(3)	0.0567(3)	0.007(1)
O(1)	0.239(1)	0.3122(9)	0.5061(9)	0.017(4)
O(2)	0.374(1)	0.1828(9)	0.5769(8)	0.010(3)
O(3)	0.063(2)	0.1976(8)	0.4204(7)	0.010(3)
O(4)	0.375(1)	0.1825(9)	0.4218(8)	0.013(3)
O(5)	0.057(2)	0.1948(8)	0.5771(7)	0.010(3)
O(6)	0.201(1)	0.0700(8)	0.5010(8)	0.009(3)
O(7)	0.198(2)	0.1997(9)	0.2332(8)	0.016(3)
O(8)	0.382(1)	0.3275(8)	0.1778(8)	0.008(3)
O(9)	0.360(2)	0.3036(9)	0.3312(9)	0.013(3)
O(10)	0.074(1)	0.3370(7)	0.1630(7)	0.005(2)
O(11)	0.051(1)	0.3162(8)	0.3214(7)	0.008(3)
O(12)	0.218(1)	0.4389(7)	0.2623(7)	0.006(2)
O(13)	0.195(1)	0.1748(7)	0.7399(7)	0.006(3)
O(14)	0.381(1)	0.2806(8)	0.8223(7)	0.007(3)
O(15)	0.363(2)	0.3036(9)	0.6683(8)	0.012(3)
O(16)	0.069(2)	0.2919(8)	0.8337(7)	0.008(3)
O(17)	0.055(1)	0.3110(8)	0.6766(7)	0.006(3)
O(18)	0.232(1)	0.4080(8)	0.7731(7)	0.008(3)
O(19)	0.198(2)	0.310(1)	− 0.0200(8)	0.016(3)
O(20)	0.055(2)	0.2049(8)	0.0795(7)	0.008(3)
O(21)	0.368(1)	0.2131(8)	0.0783(7)	0.006(3)
O(22)	0.059(1)	0.1697(8)	− 0.0763(7)	0.007(3)
O(23)	0.372(1)	0.1726(9)	− 0.0731(8)	0.009(3)
O(24)	0.208(1)	0.0733(9)	0.0242(7)	0.011(3)
O(25)	0.202(1)	0.4788(8)	0.6492(7)	0.013(3)
O(26)	0.021(1)	0.5045(8)	0.7477(8)	0.015(3)
O(27)	0.471(1)	0.0349(8)	0.0576(7)	0.009(3)
O(28)	0.256(1)	− 0.0200(8)	0.1334(7)	0.016(3)

Atomic anisotropic displacement parameters

	U_{11}	U_{22}	U_{33}	U_{12}	U_{13}	U_{23}
Mo(1)	0.0046(8)	0.0040(9)	0.006(1)	0.0004(8)	− 0.0013(8)	0.0018(7)
Mo(2)	0.0053(7)	0.0045(6)	0.0038(7)	− 0.0000(7)	− 0.0004(9)	0.0016(8)
Mo(3)	0.0044(7)	0.0056(6)	0.0026(7)	− 0.0001(7)	− 0.0005(8)	− 0.0011(9)
Mo(4)	0.0047(8)	0.0057(9)	0.004(1)	− 0.0006(8)	− 0.0004(8)	0.0019(7)
Ba(1)	0.0129(5)	0.0210(7)	0.0134(5)	− 0.0040(6)	− 0.0009(5)	− 0.0007(6)
Ba(2)	0.0130(6)	0.0113(6)	0.0130(6)	0.0016(5)	0.0047(5)	0.0013(5)
Ba(3)	0.0141(7)	0.065(1)	0.0172(7)	0.0115(8)	0.0045(6)	0.0137(8)

$P2_12_12_1$. The reflections were corrected for Lorentz and polarization effects and for absorption. The structure was solved with the heavy-atom method.

The refinement of the atomic coordinates and their anisotropic thermal factors for Ba and Mo and isotropic thermal factors for Li, P, Cl, and O led to $R = 0.040$ and $R_W = 0.034$.

Magnetic Measurements

The magnetic susceptibility of powdered samples was investigated by SQUID magnetometry from 4.5 to 120 K. The magnetic moment of the sample holder was measured in the same temperature range under the same magnetic field. The sample holder moment was then subtracted from the measured total moment.

RESULTS AND DISCUSSION

$(MoO)_4(PO_4)_6$ *Framework*

The projection of the structure of this new chlorophosphate onto the (100) plane (Fig. 1) and the partial projection along $\vec{b}$ (Fig. 2) show that the MoO_6 octahedra and the PO_4 tetrahedra form a tridimensional $(MoO)_4(PO_4)_6$ framework, with large C-shaped tunnels running along $\vec{a}$. The structure can then be described by the stacking along $\vec{b}$ of identical $[Mo_2P_2O_{12}]_\infty$ layers interconnected through "isolated" PO_4 tetrahedra. The first remarkable feature of this new framework concerns the nature of the $[Mo_2P_2O_{12}]_\infty$ layers, whose geometry is similar to that observed for the layered chlorophosphates AMoOPO$_4$Cl (3). Its projection along $\vec{b}$ (Fig. 2) shows that it consists of classical $[MoPO_8]_\infty$ chains running along [201] and [20$\bar{1}$] in which one PO_4 tetrahedron alternates with one MoO_6 octahedron. The main difference with the MoOPO$_4$Cl chlorophosphates concerns the Mo octahedra, which are "pure oxygen" MoO_6 octahedra in the present structure, whereas they are MoO_5Cl octahedra in the layer chlorophosphate AMoOPO$_4$Cl. Note that similar layers have also been identified in the tridimensional frameworks of the Mo(V) phoshate $Li_3Ba_{0.5}(MoO)_3(PO_4)_3P_2O_7$ (6) and the vanadium phosphate $Ca(VO)_2(PO_4)_2 \cdot 4H_2O$ (7). The great analogy of this layer with the perovskite must be emphasized: the arrangement of the Mo octahedra and P tetrahedra derives from a pure octahedral perovskite layer by replacing one octahedron out of two by one PO_4 tetrahedron. This close relationship with the perovskite structure is of great interest, since it suggests that many other chlorophosphates could be generated in the future based on such an arrangement. Thus, from the analysis of the structure of the $[MoP_2O_{12}]_\infty$ layers, it appears that each PO_4 tetrahedron within the layers (P_1, P_2, P_3, P_4) shares its four apices with four MoO_6 octahedra (Mo_1, Mo_2, Mo_3, Mo_4) (Fig. 2). Two successive $[Mo_2P_2O_{12}]_\infty$ layers are interconnected through isolated PO_4 tetrahedra, P_5 and P_6 (Fig. 1), in the following way: for each layer, one $[MoPO_8]_\infty$ chain out of two shares the apical corner of its octahedra with the P_5 or P_6 tetrahedra. As a result, two adjacent $[MoPO_8]_\infty$ chains running along [201] have the apical corner of their MoO_6 octahedra directed above and below the layer, respectively.

The P_5 and P_6 tetrahedra which ensure the connection between two successive $[Mo_2P_2O_{12}]_\infty$ layers have two free apices. Consequently, large tunnels are formed at the level of

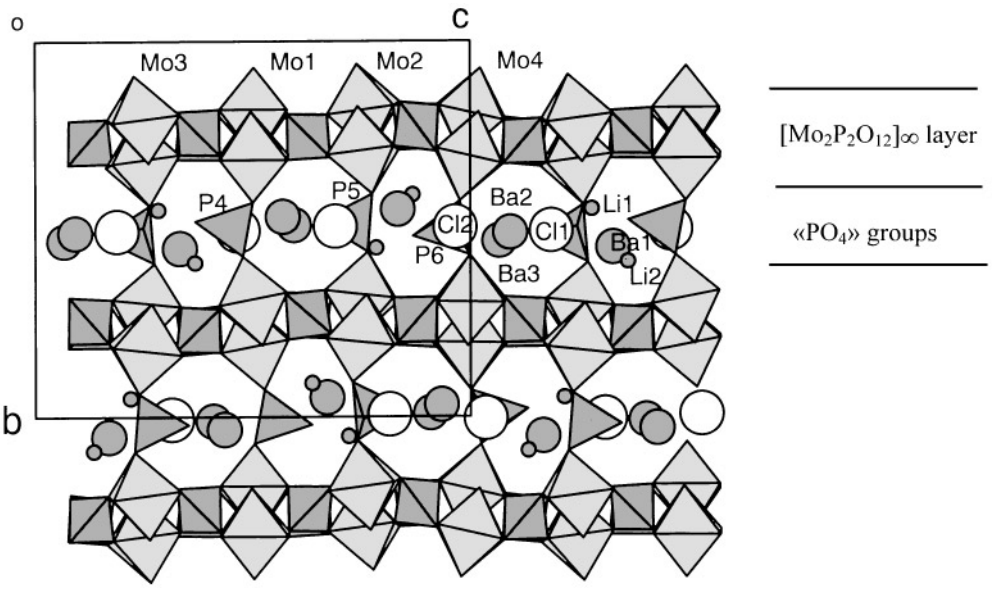

FIG. 1. Projection of the structure of $Ba_3Li_2Cl_2(MoO)_4(PO_4)_6$ along $\vec{a}$ showing the two kinds of layer.

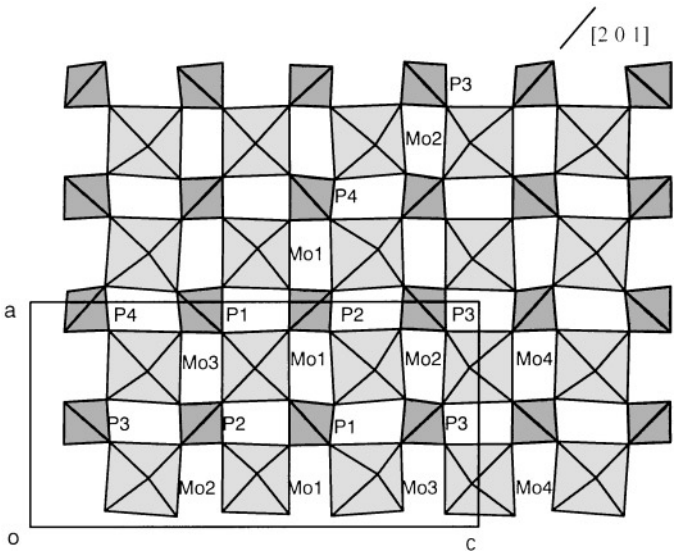

FIG. 2. The $[Mo_2P_2O_{12}]_\infty$ layer.

the P_5 and P_6 tetrahedra as shown from the C-shaped tunnels running along $\vec{a}$ (Fig. 1). In fact, this structure exhibits a pseudotetragonal symmetry ($a \cong c/2$), so that one observes C-shaped tunnels running along $\vec{c}$, similar to those parallel to $\vec{a}$. A second type of tunnel, running along [201] and [20$\bar{1}$], is also located at the level of the P_5 and P_6 tetrahedra (Fig. 3). The latter are characterized by octagonal windows built up from four MoO_6 octahedra alternating with four PO_4 tetrahedra. Thus, this molybdenyl monophosphate can be described as an intersecting tunnel structure.

The interatonic distances (Table 3) show that the PO_4 tetrahedra exhibit the classical geometry of monophosphate groups, with two shorter P–O bonds corresponding to the free apices of the P_5 and P_6 tetrahedra.

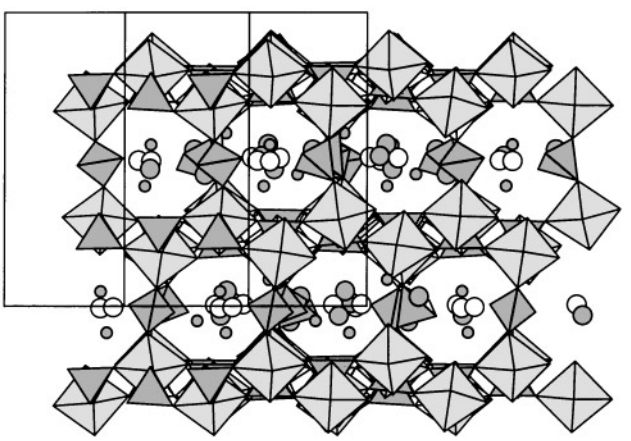

FIG. 3. Projection of the structure of $Ba_3Li_2Cl_2(MoO)_4(PO_4)_6$ along [201] showing the tunnel delimited by octagonal windows.

TABLE 3
Distances (Å) and Angles (Deg) in the Polyhedra in $Ba_3Li_2Cl_2Mo_4O_4(PO_4)_6$[a]

Mo(1)	O(1)	O(2)	O(3)	O(4)	O(5)	O(6)
O(1)	**1.68(2)**	2.70(2)	2.87(2)	2.83(2)	2.80(2)	3.81(2)
O(2)	93.3(7)	**2.02(2)**	4.03(2)	2.81(2)	2.91(2)	2.74(2)
O(3)	100.6(7)	165.7(6)	**2.04(2)**	2.88(2)	2.84(2)	2.78(2)
O(4)	97.1(7)	86.5(6)	88.4(6)	**2.08(2)**	4.06(2)	2.78(2)
O(5)	98.2(7)	92.5(6)	88.9(6)	164.7(6)	**2.01(2)**	2.73(2)
O(6)	176.0(7)	82.7(6)	83.4(5)	82.4(6)	82.3(6)	**2.14(2)**
Mo(2)	O(7)	O(8)	O(9)	O(10)	O(11)	O(12)
O(7)	**1.71(2)**	2.80(2)	2.83(2)	2.75(2)	2.78(2)	3.79(2)
O(8)	96.9(7)	**2.02(2)**	2.81(2)	2.84(2)	4.00(2)	2.77(2)
O(9)	98.7(7)	88.4(6)	**2.01(2)**	4.06(2)	2.85(2)	2.78(2)
O(10)	92.9(6)	88.0(6)	168.2(6)	**2.07(2)**	2.90(2)	2.74(2)
O(11)	96.5(6)	166.6(6)	90.4(6)	90.6(6)	**2.01(2)**	2.68(2)
O(12)	175.3(6)	84.7(5)	85.7(6)	82.8(5)	81.9(5)	**2.08(2)**
Mo(3)	O(13)	O(14)	O(15)	O(16)	O(17)	O(18)
O(13)	**1.66(2)**	2.81(2)	2.85(2)	2.76(2)	2.74(2)	3.72(2)
O(14)	98.4(6)	**2.03(2)**	2.82(2)	2.88(2)	4.02(2)	2.58(2)
O(15)	100.5(6)	88.0(6)	**2.03(2)**	4.04(2)	2.84(2)	2.78(2)
O(16)	95.3(6)	89.8(6)	164.2(6)	**2.05(2)**	2.86(2)	2.60(2)
O(17)	95.7(6)	165.9(5)	88.9(6)	89.5(6)	**2.02(2)**	2.83(2)
O(18)	172.9(6)	78.2(6)	85.7(6)	78.6(5)	87.8(5)	**2.06(2)**
Mo(4)	O(19)	O(20)	O(21)	O(22)	O(23)	O(24)
O(19)	**1.69(2)**	2.77(2)	2.82(2)	2.74(2)	2.85(2)	3.80(2)
O(20)	95.8(6)	**2.03(2)**	2.87(2)	2.88(2)	4.04(2)	2.68(2)
O(21)	99.8(6)	91.2(6)	**1.99(2)**	4.04(2)	2.82(2)	2.81(2)
O(22)	92.6(6)	88.7(6)	167.6(6)	**2.08(2)**	2.88(2)	2.73(2)
O(23)	99.2(6)	164.9(6)	88.6(6)	88.3(6)	**2.05(2)**	2.79(2)
O(24)	172.8(6)	80.6(6)	86.5(5)	81.2(5)	84.3(6)	**2.12(2)**

P(1)	O(2)	O(3^i)	O(15)	O(11^i)
O(2)	**1.52(2)**	2.55(2)	2.46(2)	2.52(2)
O(3^i)	111.7(8)	**1.55(2)**	2.59(2)	2.44(2)
O(15)	107.3(8)	113.4(8)	**1.56(2)**	2.55(2)
O(11^i)	109.8(8)	102.8(8)	111.8(8)	**1.53(2)**
P(2)	O(4)	O(5^i)	O(9)	O(17^i)
O(4)	**1.54(2)**	2.54(2)	2.51(2)	2.43(2)
O(5^i)	110.9(8)	**1.51(2)**	2.46(2)	2.56(2)
O(9)	111.3(8)	107.1(8)	**1.55(2)**	2.54(2)
O(17^i)	103.8(8)	112.1(8)	111.7(8)	**1.55(2)**
P(3)	O(8)	O(16^i)	O(21)	O(22^{ii})
O(8)	**1.52(2)**	2.54(2)	2.54(2)	2.46(2)
O(16^i)	112.1(7)	**1.55(2)**	2.44(2)	2.52(2)
O(21)	112.6(8)	104.4(8)	**1.54(2)**	2.54(2)
O(22^{ii})	106.9(8)	109.4(8)	111.4(7)	**1.54(2)**
P(4)	O(10^i)	O(14)	O(20^i)	O(23^{iii})
O(10^i)	**1.54(2)**	2.57(2)	2.57(2)	2.47(2)
O(14)	112.6(7)	**1.54(2)**	2.40(2)	2.54(2)
O(20^i)	111.5(8)	101.4(8)	**1.56(2)**	2.55(2)
O(23^{iii})	107.4(8)	112.2(8)	111.8(8)	**1.52(2)**

TABLE 3—*Continued*

P(5)	O(12^{iv})	O(18)	O(25)	O(26)
O(12^{iv})	**1.55(2)**	2.45(2)	2.53(2)	2.57(2)
O(18)	102.7(7)	**1.58(2)**	2.52(2)	2.50(2)
O(25)	111.1(7)	108.6(7)	**1.52(2)**	2.47(2)
O(26)	115.2(7)	108.7(7)	110.2(8)	**1.49(2)**
P(6)	O(6^{v})	O(24)	O(27)	O(28)
O(6^{v})	**1.55(2)**	2.43(2)	2.50(2)	2.55(2)
O(24)	103.2(7)	**1.55(2)**	2.56(2)	2.50(2)
O(27)	108.2(7)	112.4(8)	**1.53(2)**	2.55(2)
O(28)	111.7(8)	108.3(8)	112.7(8)	**1.53(2)**

Ba(1)–O(28^{i})	= 2.64(2)	Ba(2)–O(25^{i})	= 2.62(2)
Ba(1)–O(18)	= 2.80(2)	Ba(2)–O(4)	= 2.77(2)
Ba(1)–O(14)	= 2.87(2)	Ba(2)–O(24^{vi})	= 2.83(2)
Ba(1)–O(20^{i})	= 2.93(2)	Ba(2)–O(22^{vi})	= 2.84(2)
Ba(1)–O(12^{iv})	= 2.98(2)	Ba(2)–O(6)	= 2.92(2)
Ba(1)–O(7^{i})	= 3.14(2)	Ba(2)–O(26^{i})	= 2.92(2)
Ba(1)–Cl(2^{iv})	= 2.971(2)	Ba(2)–Cl(1)	= 3.075(6)
Ba(1)–Cl(1^{i})	= 3.057(6)	Ba(2)–Cl(2^{i})	= 3.121(6)
Ba(3)–O(25)	= 2.53(2)	Li(1)–O(26^{viii})	= 1.78(4)
Ba(3)–O(27^{vii})	= 2.67(2)	Li(1)–O(28^{vi})	= 1.85(4)
Ba(3)–O(6^{i})	= 2.88(2)	Li(1)–O(13)	= 2.05(4)
Ba(3)–O(3^{i})	= 2.89(2)	Li(1)–Cl(1^{vi})	= 2.63(4)
Ba(3)–O(1)	= 3.16(2)		
Ba(3)–O(15)	= 3.20(2)	Li(2)–O(27^{ix})	= 1.91(6)
Ba(3)–Cl(2)	= 3.066(6)	Li(2)–O(16)	= 1.94(6)
Ba(3)–Cl(1^{i})	= 3.116(6)	Li(2)–O(18)	= 2.19(6)
		Li(2)–O(26)	= 2.65(6)

[a]Symmetry codes: i = $1/2 + x, 1/2 - y, 1 - z$; ii = $1/2 + x, 1/2 - y, -z$; iii = $x, y, 1 + z$; iv = $1/2 - x, 1 - y, -1/2 + z$; v = $1/2 - x, -y, -1/2 + z$; vi = $1/2 - x, -y, 1/2 + z$; vii = $1 - x, 1/2 + y, 1/2 - z$; viii = $-x, -1/2 + y, 3/2 - z$; ix = $-1/2 + x, 1/2 - y, 1 - z$.

The geometry of the MoO_6 octahedra is characteristic of Mo(V). One observes a short Mo–O bond, ranging from 1.66 to 1.71 Å, opposed to a larger one (2.06–2.14 Å), which both correspond to the apical apices. The four equatorial Mo–O bonds are intermediate, ranging from 1.99 to 2.08 Å (Table 3). The bond valence calculations, performed for the molybdenum using the Brese and O'Keeffe (8) expression, confirm the pentavalent character of molybdenum. The bond valence parameters have been refined to $R_{ij} = 1.879$ on the basis of the data obtained from 86 Mo(V) octahedra of various structures and lead to calculated valences of 4.81, 4.84, 5.05, and 4.80 for Mo(1), Mo(2), Mo(3), and Mo(4), respectively.

The Interpolated Species: Ba^{2+}, Li^{+}, and Cl^{-}

The Ba^{2+} and Li^{+} cations and Cl^{-} anions sit in the tunnels at the level of the P_5 and P_6 tetrahedra (Figs. 1 and 3). The distribution of these different species can be better understood by considering one (010) layer (Fig. 4). It can be seen that these anions and cations form approximately straight rows running along [201] and [20$\bar{1}$], the full lines corresponding approximately to the axis of the tunnels, with the sequence $[(Ba–Cl)_3(Li \ldots Li–Cl)_1]$. Note that the Cl^{-} anions sit at the intersection of one [201] and one [20$\bar{1}$] tunnel. The Ba^{2+} cations form approximately straight rows running along [100] and [001] (the dashed lines correspond to the axis of the tunnels). They sit approximately at the intersection of the [100] and [001] and [201] or [20$\bar{1}$] tunnels. The Li^{+} cations are located in the [100] and [201] tunnels between two Cl^{-} anions (see full lines in Fig. 4).

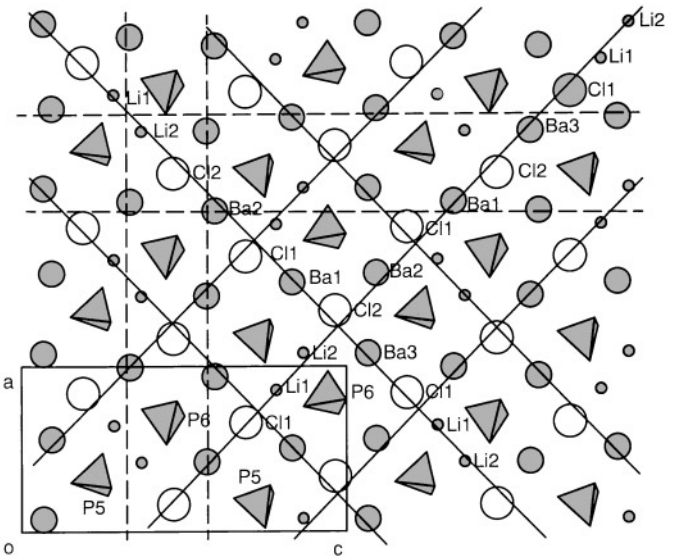

FIG. 4. Sitting of Ba^{2+}, Li^{+}, and Cl^{-} species in the "PO_4" layers.

The lithium coordination suggests two comments. As shown in Fig. 5, Li(1) exhibits a tetrahedral coordination,

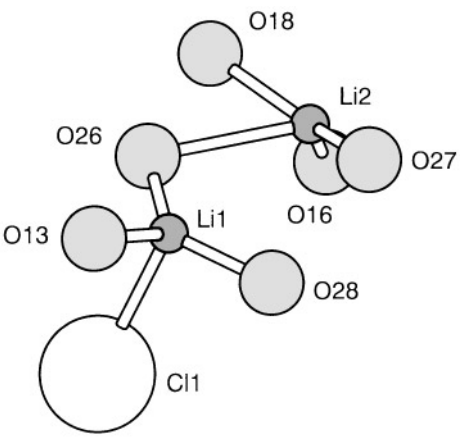

FIG. 5. Coordination of the Li cations.

corresponding to the unit LiO_3Cl, with Li–O and Li–Cl distances (Table 3) close to those generally observed. In contrast, Li(2) exhibits a particular behavior with three nearest oxygen atoms located at 1.91–2.19 Å and a fourth oxygen atom much further (2.63 Å). Thus the coordination of Li(2) can be described either as a triangular LiO_3 group or as a distorted flattened tetrahedron LiO_4 (Fig. 5). Note that this fourth neighbor corresponds to the bridging oxygen atom (O(26)) between Li(1) and Li(2).

Each Ba^{2+} cation is surrounded by six oxygen atoms with Ba–O bonds ranging from 2.53 to 3.20 Å and two chlorine atoms with Ba–Cl bonds ranging from 2.971 to 3.121 Å delimiting dodecahedra.

Magnetic Properties

A small amount (~ 0.050 g) of crystals was extracted from the polyphasic samples. The magnetic moment was measured by SQUID magnetometry. The sample was first zero field cooled to $T = 4.5$ K. The magnetic field ($B = 0.3$ T) was then applied and the magnetic susceptibility $\chi_m(T)$ ($T > 75$ K) measured. The data were fit with a Curie–Weiss law:

$$\chi_m = \chi_0 + \frac{C}{T - \theta}$$

The fitting parameter C leads to a paramagnetic moment of 1.46 μ_B per Mo(V), which is lower than the theoretical value for a d^1 isolated ion (1.73 μ_B).

The low-temperature range of the molar susceptibility $\chi_m(T)$ ($4.5 < T < 120$ K) is shown in Fig. 6. The magnetic behavior of $Ba_3Li_2Cl_2(MoO)_4(PO_4)_6$ in the low-temperature range is complex. A first rounded peak is observed at $T = 20$ K and a sharper second one at $T = 10$ K. The measurements were performed on two selections of single crystals carefully extracted from two different preparations and the experimental results are perfectly reproducible. Thus, at first glance, it seems difficult to invoke an impurity contribution to explain the sharp peak at $T = 10$ K.

The results suggest low-dimensional antiferromagnetic behavior for $10 < T < 20$ K. Such a phenomenon can be explained by the particular geometry of the structure, which consists of $[Mo_2P_2O_{12}]_\infty$ layers interconnected through PO_4 tetrahedra along $\vec{b}$. Within each $[Mo_2P_2O_{12}]_\infty$ layer, an antiferromagnetic coupling between molybdenum atoms can be proposed, due to the fact that the equatorial Mo–O bonds are rather short, forming $[Mo–O–P–O–Mo]_\infty$ rows along [201] and $[20\bar{1}]$. Such an antiferromagnetic coupling may result in a square array of alternating up and down neighboring spins. Considering these Mo(V) rows (Fig. 2), two successive chains are located at a different level along $\vec{b}$, and it is indeed possible that one [201] row exhibits the spin-up configuration whereas the next one exhibits the spin-down configuration. In contrast, no $[Mo–O–P–O–Mo]_\infty$ chain is observed along $\vec{b}$. Only "Mo–O–P–O–Mo" dimers can be seen (Fig. 1). Moreover, the Mo–O bonds are significantly larger than in the layers, in agreement with the formation of the opposite abnormally short molybdenyl

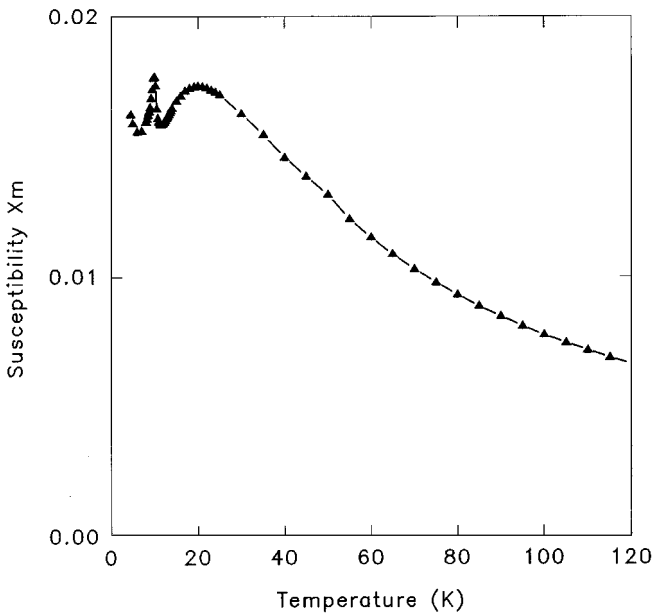

FIG. 6. Molar magnetic susceptibility $\chi_m(T)$ versus temperature T in the range $4.5 \leq T \leq 120$ K.

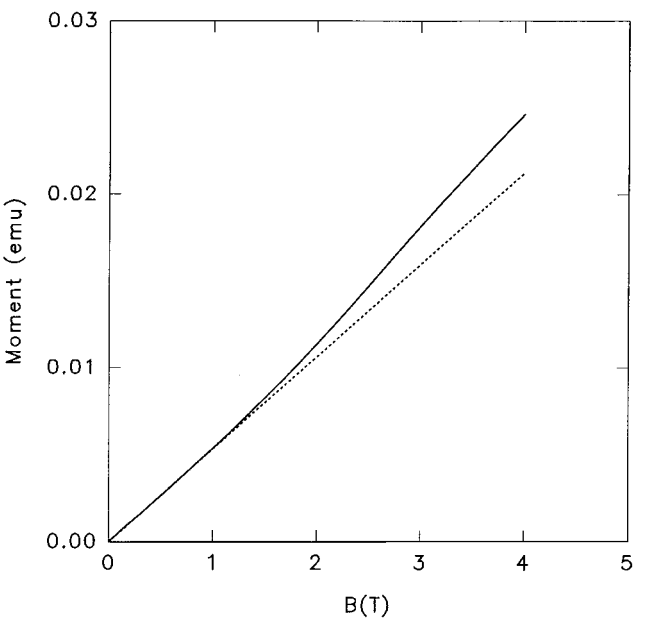

FIG. 7. Magnetic moment at $T = 4.5$ K versus magnetic field $M(H)$. The dotted line is the low-field slope of $M(H)$.

bond. Consequently, with such a bond alternation, the d^1 electron tends to occupy the $d_{x^2-y^2}$ orbitals within the $[Mo_2P_2O_{12}]_\infty$ layers, leaving the d_{z^2} orbitals empty along $\vec{b}$. This situation is detrimental to the occurrence of magnetic coupling along $\vec{b}$ between two successive $[Mo_2P_2O_{12}]_\infty$ layers.

The peak at 10 K on the $\chi(T)$ curve may be related to canting phenomena, if one bears in mind that the MoO_6 octahedra are tilted along the lower and upper rows. The $M(B)$ curve, registered at 4.5 K (Fig. 7), supports this viewpoint. One observes that the slope is increasing for $B > 1$ T as compared to the initial slope shown as a dotted line. At $T = 20$ and 50 K, $M(B)$ is linear up to 4 T without any change in the slope. Neutron diffraction studies will be necessary to check this hypothesis. To date, we have not succeeded in synthesizing a sufficient amount of single-phase crystals to perform such measurements.

In conclusion, a new Mo(V) chlorophosphate has been synthesized whose close relationships with the perovskite structure open the route to the generation of other Mo(V) oxychlorides. The low-dimensional antiferromagnetic properties of this new phase below 20 K, although they have to be confirmed, are of interest to understand the peculiar behavior of Mo(V).

REFERENCES

1. G. Costentin, A. Leclaire, M.-M. Borel, A. Grandin, and B. Raveau, *Rev. Inorg. Chem.* **13,** 77 (1993).
2. R. C. Haushalter and L. A. Mundi, *Chem. Mater.* **4,** 31 (1992).
3. M.-M. Borel, A. Leclaire, J. Chardon, J. Provost, and B. Raveau, *J. Solid State Chem.* **137,** 214 (1998).
4. M.-M. Borel, J. Chardon, A. Leclaire, A. Grandin, and B. Raveau, *J. Solid State Chem.* **112,** 317 (1994).
5. G. Costentin, M.-M. Borel, A. Grandin, A. Leclaire, and B. Raveau, *J. Solid State Chem.* **89,** 83 (1990).
6. S. Ledain, A. Leclaire, M. M. Borel, M. Hervieu, J. Provost, and B. Raveau, *J. Solid State Chem.* (submitted).
7. H.Y. Kang, N.C. Lee, and S.L. Wang, *Inorg. Chem.* **31,** 4743 (1992).
8. N.E. Brese and M.O. Keeffe, *Acta Crystallogr., Sect. B* **47,** 129 (1991).
9. E. Canadell, J. Provost, A. Guesdon, M.-M. Borel, and A. Leclaire, *Chem. Mater.* **9,** 68 (1997).